ЖЭТФ, 2016, том 150, вып. 1 (7), стр. 144–150

MAGNETIC PROPERTIES OF $(SrFe_{12}O_{19})_x(CaCu_3Ti_4O_{12})_{1-x}$ COMPOSITES

R. M. Eremina [a,b*], *K. R. Sharipov* [a], *I. V. Yatsyk* [a,b], *N. M. Lyadov* [a], *I. F. Gilmutdinov* [b], *A. G. Kiiamov* [b], *Yu. V. Kabirov* [c], *V. G. Gavrilyachenko* [c], *T. I. Chupakhina* [d]

[a] *Zavoisky Physical-Technical Institute, 420029, Kazan, Russia*

[b] *Kazan Federal University, 420008, Kazan, Russia*

[c] *Southern Federal University, 344006, Rostov-on-Don, Russia*

[d] *Institute of Solid State Chemistry, Ural Branch, Russian Academy of Sciences 620990, Ekaterinburg, Russia*

Received December 27, 2015

New composite materials $(SrFe_{12}O_{19})_x(CaCu_3Ti_4O_{12})_{1-x}$ ($x = 0$, 0.05, 1) have been synthesized. Their magnetic properties are studied in the temperature range 5–300 K using the magnetic resonance and magnetometry methods. It is found that strontium hexaferrite micro inclusions in the $(SrFe_{12}O_{19})_{0.05}(CaCu_3Ti_4O_{12})_{0.95}$ composite "magnetize" $CaCu_3Ti_4O_{12}$ at temperatures from 300 to 200 K, forming a ferrimagnetic particle near the $SrFe_{12}O_{19}$ "core". The magnetic resonance line below 200 K splits into two lines corresponding to $SrFe_{12}O_{19}$ and $CaCu_3Ti_4O_{12}$. The core effect decoration is manifested in the increase in the Curie–Weiss temperature from 25 K in $CaCu_3Ti_4O_{12}$ without the doping ceramics to 80 K in the composite with 5 % of $SrFe_{12}O_{19}$.

DOI: 10.7868/S0044451016070130

1. INTRODUCTION

Composite materials attract much attention because they exhibit unexpected new physical properties [1]. The most interesting are composite compounds formed by combinting materials with high values of the magnetic susceptibility and dielectric permittivity. Hexaferrites, in particular, strontium hexaferrite (M-ferrite) $SrFe_{12}O_{19}$ (SFO), are often used among possible magnetic single-phase materials [2]. Strontium hexaferrite $SrFe_{12}O_{19}$ has the structure of a magnetoplumbite with the space group $P6_3/mmc$, the cell parameters $a = b = 5.87$ Å and $c = 23.00$ Å, and the temperature of the phase transition to the ferrimagnetic state $T_C = 737$ K [3, 4]. The dielectric permittivity ε' varies from 10^4 to 10^1 in the frequency range 10^{-3}–10^7 Hz [5]. The $CaCu_3Ti_4O_{12}$ (CCTO) compound with a perovskite-type structure and the space group $Im\bar{3}$, $a = 0.7391$ nm, undergoes a phase transition into the antiferromagnetically ordered phase below 25 K and has a high value of the dielectric permittivity $\varepsilon \sim 10^4$–10^5 in a wide temperature range (100–600 K) for frequencies up to 10 MHz [6, 7]. The results of investigations of polycrystalline CCTO samples using the method of electron paramagnetic resonance (EPR) are given in Refs. [8, 9]. In Ref. [9], samples were annealed in different gases: air, argon, or oxygen. It was established that the value of the effective g-factor is approximately 2.15 and is independent of the annealing atmosphere, while the value of the linewidth varies considerably with the change in the oxygen content.

In this paper, we study the magnetic properties of SFO- and CCTO-based composites prepared according to the specific "core-shell" technology by the magnetic resonance and magnetometry methods.

2. SAMPLES AND THEIR CHARACTERIZATION

Ceramic $SrFe_{12}O_{19}$ and $CaCu_3Ti_4O_{12}$ samples were synthesized according to the standard ceramic technology using oxides Fe_2O_3, TiO_2, and CuO and calcium and strontium carbonates of a special purity grade.

* E-mail: REremina@yandex.ru

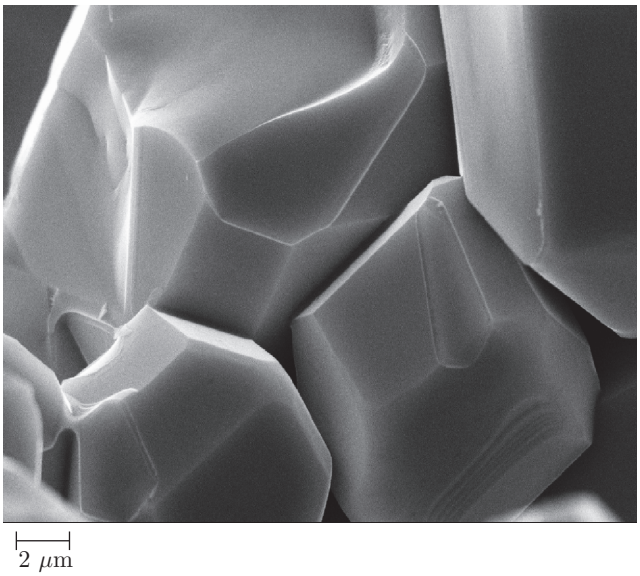

Fig. 1. A scanning electron microscopy (SEM) image of the surface of the sample $(SrFe_{12}O_{19})_{0.05}(CaCu_3Ti_4O_{12})_{0.95}$

To prepare composites with 5 mass. % strontium hexaferrite and 95 mass. % $CaCu_3Ti_4O_{12}$, preliminarily synthesized strontium hexaferrite was added to the stoichiometric mixture of oxides $CaO{:}3CuO{:}4TiO_2$. After the materials were homogenized, tablets with the diameter of 8 mm and thickness of 2 mm were pressed under the pressure of 50 MPa. The sintering time at the temperature of 1100 °C was 3 h for all samples.

The microstructure of $(SrFe_{12}O_{19})_{0.05}(CaCu_3Ti_4O_{12})_{0.95}$ composite was studied with an EVO SOXVP electron scanning microscope with microanalysis (Carl Zeiss). The X-ray fluorescence analyses (XFA) of $(SrFe_{12}O_{19})_{0.05}(CaCu_3Ti_4O_{12})_{0.95}$ was carried out with the Bruker S2 Ranger X-ray fluorescence spectrometer at room temperature. Powder diffraction patterns of $(SrFe_{12}O_{19})_{0.05}(CaCu_3Ti_4O_{12})_{0.95}$ were obtained as a result of detection in the symmetric Bragg–Brentano geometry with a D8 Advance X-ray diffractometer (Bruker) using an X-ray tube with a copper anode at the detection rate of 0.002 degree/s in the range of 2Θ angles of 15–80 degrees with a step of 0.015 degree.

Magnetic resonance spectra of the composites were measured with an ER 200 SRC (EMX/plus) spectrometer (Bruker) at the frequency of 9.4 GHz in the temperature range 100–300 K. The temperature dependence of the magnetization was measured with a PPMS-9 device in the temperature range 4–300 K.

Features of the formation of the $(SrFe_{12}O_{19})_{0.05}(CaCu_3Ti_4O_{12})_{0.95}$ composite were studied using SEM. The SEM image of the surface of the $(SrFe_{12}O_{19})_{0.05}(CaCu_3Ti_4O_{12})_{0.95}$ composite is shown in Fig. 1. SEM images indicate that unlike the cubic habitus pure $CaCu_3Ti_4O_{12}$, the shape of crystallites is distorted considerably, which is associated with the feature of their growth on hexagonal $SrFe_{12}O_{19}$ seeds. The sizes of crystallites range from 4 to 10 μm.

The element distribution was obtained by the microprobe analysis in different points of the sample $(SrFe_{12}O_{19})_{0.05}(CaCu_3Ti_4O_{12})_{0.95}$. The average values are presented in Table 1.

The microanalysis was performed without the oxygen reference; therefore, the average content values of atoms can differ from the values claimed during the synthesis. The obtained values coincide with the stated stechiometry with the accuracy of experimental error, obtained as the standard deviation from the mean of fifteen experimental points.

We have also investigated $(SrFe_{12}O_{19})_{0.05}(CaCu_3Ti_4O_{12})_{0.95}$ by an additional X-ray fluorescence analysis method. The XFA image is shown in Fig. 2, where bright areas correspond to the regions with *a*) Fe and *b*) Sr. Strontium hexferrite in the composite has the shape of an elongated cylinder as shown in Fig. 2*b*. The components of the composite are uniformly distributed across the sample according to the X-ray fluorescent analysis.

The precision X-ray phase analysis of $(SrFe_{12}O_{19})_{0.05}(CaCu_3Ti_4O_{12})_{0.95}$ ceramics was conducted. The diffraction pattern taken with a long exposure time in a point at room temperature contains no reflexes referring to iron or strontium oxides. Figure 3 shows experimental and theoretical diffraction patterns of the $(SrFe_{12}O_{19})_{0.05}(CaCu_3Ti_4O_{12})_{0.95}$ composite processed on the basis of structural data referring to $CaCu_3Ti_4O_{12}$ (the space group $Im\bar{3}$, № 204). In addition to the main phase, the diffraction pattern contains very weak reflexes referring to $SrFe_{12}O_{19}$. The lattice parameters were specified using the full profile analysis in the Fullprof 2014 program medium. The parameter values are as follows: $a = 7.39447(11)$ Å, the R_f-factor is 1.03, $R_B = 2.09$, and $\chi^2 = 4.01$.

3. MAGNETIC PROPERTIES

The temperature dependence of the magnetization of $(SrFe_{12}O_{19})_{0.05}(CaCu_3Ti_4O_{12})_{0.95}$ was studied in the temperature range 4–300 K. Figure 4*a* shows the temperature dependence of the quantity H/M of

Table 1. Average content of the $(SrFe_{12}O_{19})_{0.05}(CaCu_3Ti_4O_{12})_{0.95}$ composite obtained using the EVO SOXVP microanalysis

	Sr	Fe_{12}	O_{19}	Ca	Cu_3	Ti_4	O_{12}
Average	0.93	12.3	20.7	0.83	2.68	3.13	12.48
Experimental error	0.18	1.9	1.6	0.16	0.55	0.84	0.96

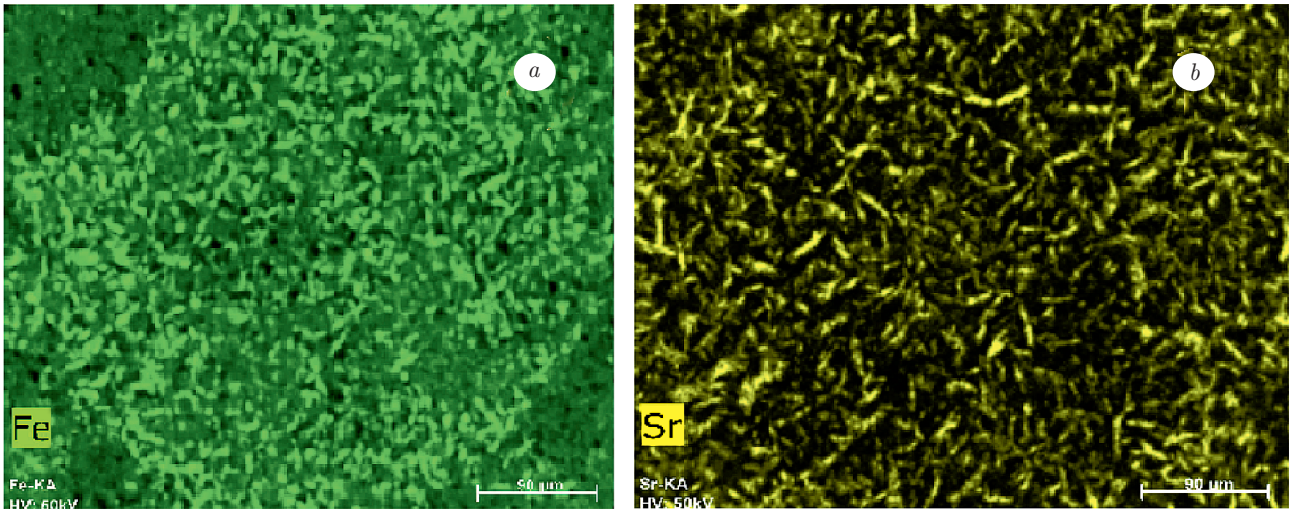

Fig. 2. Maps of element distributions in a sample of the $(SrFe_{12}O_{19})_{0.05}(CaCu_3Ti_4O_{12})_{0.95}$ composite: *a*) Fe, *b*) Sr (XFA image)

Table 2. Fitting parameters of the temperature dependence of the $(SrFe_{12}O_{19})_{0.05}(CaCu_3Ti_4O_{12})_{0.95}$ magnetic susceptibility by the Curie–Weiss law $\chi^{-1} = C^{-1}(T - \theta_{CW})$

Temperature region, K	C, K·CGCM/mol	θ_{CW}, K	μ_{eff}, μ_B
1 ($T < 25$ K)	10	−27	8.94
2 (25 K $< T <$ 220 K)	107	−470	29.26
3 ($T > 220$ K)	49	−80	19.79

the $(SrFe_{12}O_{19})_{0.05}(CaCu_3Ti_4O_{12})_{0.95}$ composite measured in the field of 1000 Oe. The temperature dependence of the magnetic susceptibility is described by three linear regions following the Curie–Weiss law $\chi^{-1} = C^{-1}(T - \theta_{CW})$ with different values of the constant C and the Curie–Weiss temperature. The constant C and θ_{CW} values for three regions are given in Table 2.

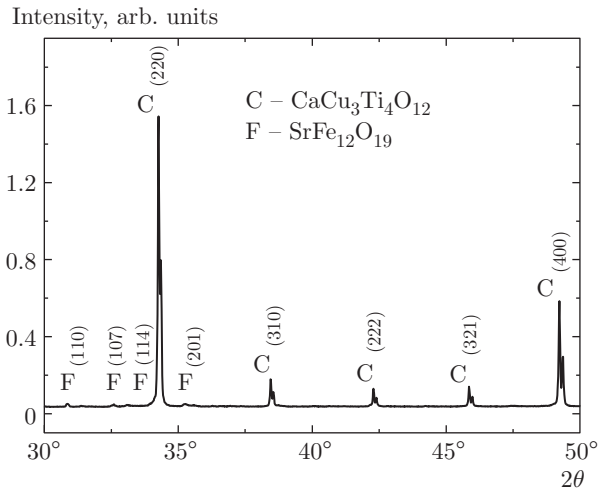

Fig. 3. A diffraction pattern $(SrFe_{12}O_{19})_{0.05}(CaCu_3Ti_4O_{12})_{0.95}$ at room temperature

In the temperature dependence, we can see kinks at temperatures of approximately 25 and 220 K. The magnetic susceptibility of the composite is the sum of three contributions: *a*) from the ferromagnetic 5 %

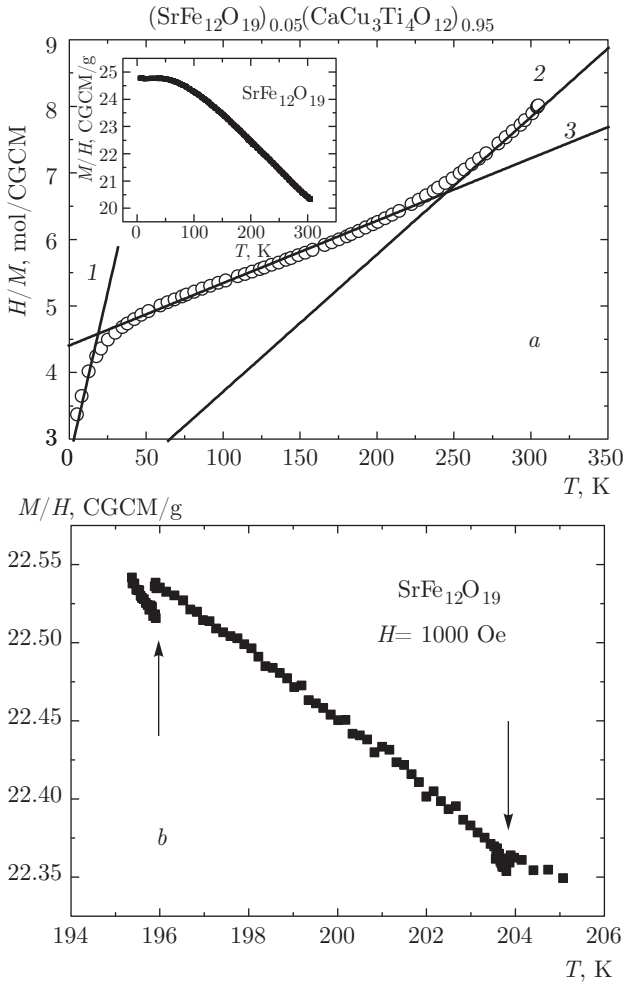

Fig. 4. *a*) The temperature dependence of H/M for the $(SrFe_{12}O_{19})_{0.05}(CaCu_3Ti_4O_{12})_{0.95}$ composite, *b*) temperature dependences of quantity M/H for $SrFe_{12}O_{19}$ in the range of 200 K, where two kinks were observed. Inset: temperature dependences of quantity M/H for $SrFe_{12}O_{19}$

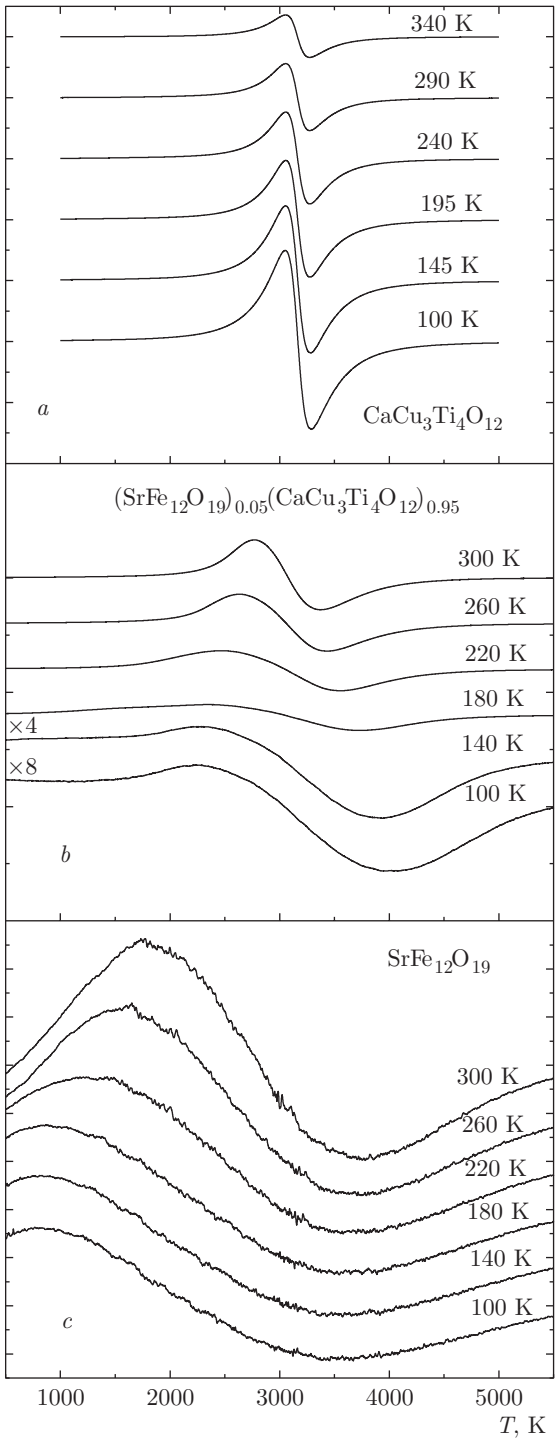

Fig. 5. The evolution of EPR spectra with temperature and composition in *a*) $CaCu_3Ti_4O_{12}$, *b*) $(SrFe_{12}O_{19})_{0.05}(CaCu_3Ti_4O_{12})_{0.95}$, *c*) $SrFe_{12}O_{19}$

SFO, which is almost independent of the temperature below 46 K; *b*) from the 95 % CaCuTiO subsystem located far from the "core" SFO, which is antiferromagnetically ordered below 25 K; *c*) from the paramagnetic region located on the border between CaCuTiO and SrFeO, which grows with decreasing the temperature. The increase in magnetization below 25 K is connected with the region near the "core", which has a paramagnetic state. The kink of the magnetization temperature dependence near 220 K is accompanied by line splitting in the magnetic resonance spectrum of this composite (see Fig. 5), which we discuss in detail below.

The effective magnetic moment in each temperature range was estimated from the formula $\mu_{eff} = \sqrt{3k_BC/N_A}$, where C is the Curie–Weiss constant,

k_B is the Boltzmann constant, and N_A is the Avogadro number. It can be seen from Table 2 that the effective magnetic moment varies as a function of the temperature range. The analysis of the temperature dependence of the magnetic susceptibility given below is somewhat conventional, because, according to magnetic resonance data, the phase stratification is observed in the $(SrFe_{12}O_{19})_{0.05}(CaCu_3Ti_4O_{12})_{0.95}$ composite below 200 K, and $SrFe_{12}O_{19}$ has the ferrimagnetically ordered state below approximately 737 K. The magnetic moment is proportional to the sample mass, and the coefficients 0.05 and 0.95 in the formula $(SrFe_{12}O_{19})_{0.05}(CaCu_3Ti_4O_{12})_{0.95}$ refer to the structural units. We calculate the percent mass ratio of composites. The molar mass is 1061.7486 g/mol for SFO and 620.1768 g/mol for CCTO. The mass ratio in the $(SFO)_{0.05}(CCTO)_{0.95}$ composite is 0.083 for SFO and 0.917 for CCTO. We compare the effective moment μ_{eff} with the theoretical paramagnetic moment of spins of iron and copper ions according to the formula $\mu_{eff}^2 = (1-y)\mu_{\text{Fe}}^2 + y\mu_{\text{Cu}}^2$ [10] in different temperature ranges. In $SrFe_{12}O_{19}$ ceramics, the Fe^{3+} ion with the spin $S = 5/2$ is magnetic, which is in the intermediate ligand field in the octahedral field, $g_{\text{Fe}} \approx 2$. We calculate the value of the effective magnetic moment in the range 200–300 K. The effective magnetic moment in the paramagnetic phase is given by $\mu = \sqrt{ZS(S+1)}\, g\mu_B$, where Z is the number of ions with spin S in the chemical formula. For SFO, $Z_{\text{Fe}} = 12$, and $g_{\text{Fe}} \approx 2$ for CCTO with $Z_{\text{Cu}} = 3$ and $g_{\text{Cu}} \approx 2.15$, whence

$$\mu_{eff} = \mu_B \times$$
$$\times \sqrt{g_{\text{Fe}}^2(1-y)Z_{\text{Fe}}S_{\text{Fe}}(S_{\text{Fe}}+1)+g_{\text{Cu}}^2 y Z_{\text{Cu}}S_{\text{Cu}}(S_{\text{Cu}}+1)} =$$
$$= 6.38\mu_B.$$

The calculated value of the effective magnetic moment is much less than the experimental one in the temperature range 200–300 K. This can be associated with the strong polarization of spins of copper ions of the CCTO shell at the SFO boundary "core". On the other hand, SFO is ordered ferrimagnetically, and therefore the presented estimate of the effective magnetic moment is rough. The composition effect from the addition of 5 % SFO during the CCTO synthesis is manifested in the increase in the absolute value of the Curie–Weiss temperature from 25 to 80 K in comparison with that of the initial CCTO compound. The question about the nature of the exchange interaction between spins of copper and iron ions at the core–shell boundary remains open. It is rather difficult to unambiguously assert the character of the exchange interactions between spins at the boundary between the SFO and the CCTO. According to the Goodenough–Kanamori rule, the value and character of the indirect exchange interaction (ferromagnetic or antiferromagnetic) depend on the mutual location of magnetic ions and ligands. The magnetic structure of strontium hexaferrite is very complex; iron ions occupy positions $2a$, $2b$, $12k$, $4f_1$, $4f_2$ [11] with different ligand environments, and the character of the exchange interaction between copper ions CCTO at the boundary with SFO can differ. For example, multiferroic $YBaCuFeO_5$ is a good example of how the character and the value of exchange interactions between Fe^{3+} and Cu^{2+} spins vary [12]. Iron and copper ions in this compound are surrounded by oxygen ions, which form FeO_5 and CuO_5 bipyramids. The temperature dependence of the magnetic susceptibility reveals two phase transitions at the temperatures $T_{N1} \approx 440$ K and $T_{N2} \approx 200$ K. Possible variants of the distribution of iron and copper ions in bipyramids are considered in [12]. It is shown that the value and sign of the exchange interaction differ as a function of the ways of the indirect exchange interaction between spins of copper and iron ions (see Table II in Ref. [12]).

Figures 4*a* (inset) and 4*b* show the temperature dependence of M/H measured in the field of 1000 Oe for the $SrFe_{12}O_{19}$ compound. The shape of the temperature dependence and the relevant values are in agreement with the literature data [11, 13]. The magnetization is temperature-independent below 46 K, where all sublattices of spins of Fe^{3+} ions are completely ordered. In Fig. 4*b*, the region near 200 K is singled out, in which two kinks probably associated with the ordering of one of the sublattices of iron ions in $SrFe_{12}O_{19}$ are observed.

A single rather narrow line is observed in EPR spectra of $CaCu_3Ti_4O_{12}$ in the temperature range 100–300 K (see Fig. 5*a*). The resonance field value, the (peak-to-peak) linewidth, and the integral intensity obtained by double integration of the line are given in Fig. 6 (squares). The value of the EPR linewidth in $CaCu_3Ti_4O_{12}$ ceramics is approximately 200 Oe at room temperature and is in agreement with data given in Refs. [8, 9]. The temperature dependence of the integral intensity of the magnetic resonance line in $CaCu_3Ti_4O_{12}$ is approximated satisfactorily by the Curie–Weiss law. The solid line in Fig. 6*c* corresponds to $\chi = C/(T - \theta_{CW})$, where θ_{CW} is the Curie–Weiss temperature, which is approximately -25 K, in agreement with the literature data [8]. The experimental intensity data are divided by intensity value at $T = 300$ K.

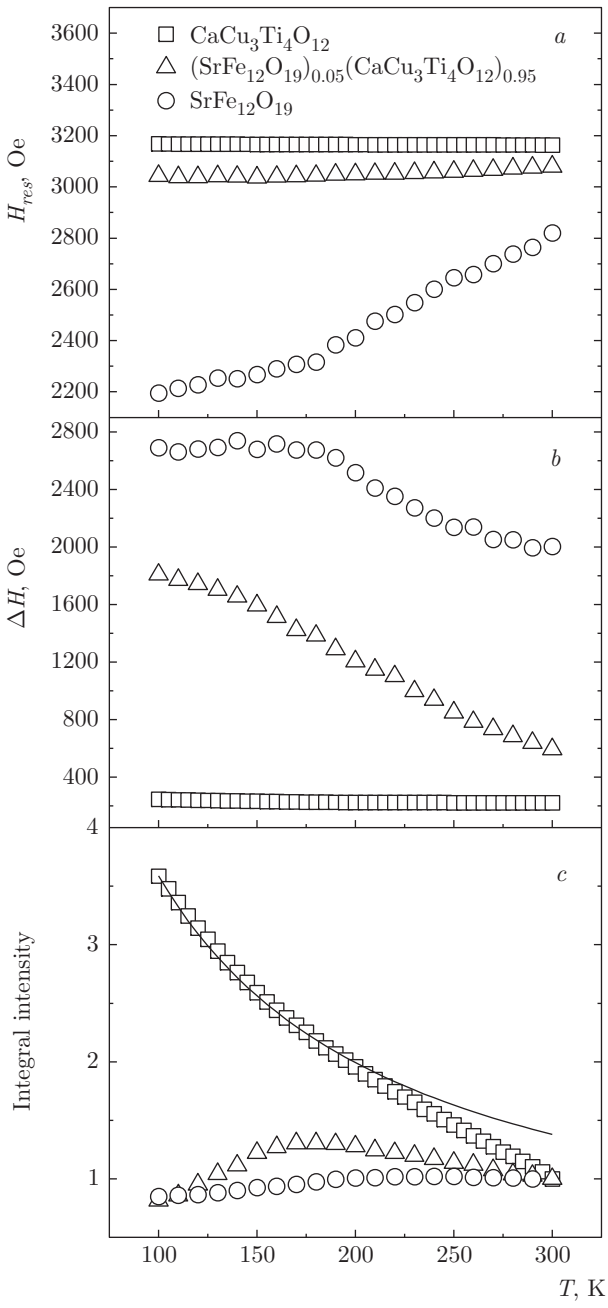

Fig. 6. Temperature dependences of (a) the resonance field value, (b) the linewidth (peak-to-peak), and (c) the integral intensity was obtained by double integration of the magnetic resonance line for $CaCu_3Ti_4O_{12}$. The solid line is the Curie–Weiss low $\chi = C/(T - \theta_{CW})$

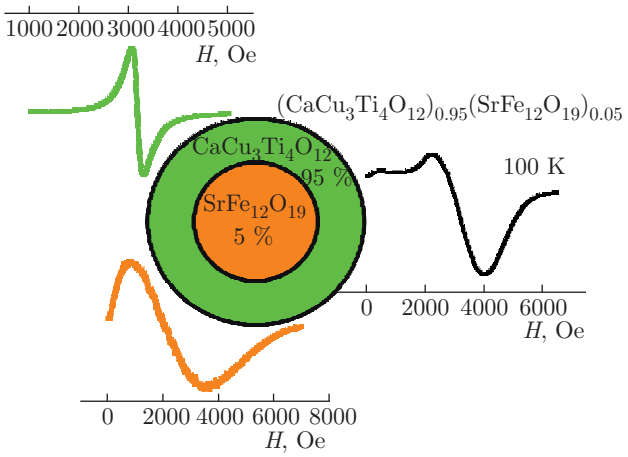

Fig. 7. The model "core–shell" of $(SrFe_{12}O_{19})_{0.05}(CaCu_3Ti_4O_{12})_{0.95}$

The shape of the magnetic resonance spectrum and its characteristics were changed considerably in the $(SrFe_{12}O_{19})_{0.05}(CaCu_3Ti_4O_{12})_{0.95}$ composite (see Fig. 5b). We note that two lines are observed in the $(SrFe_{12}O_{19})_{0.05}(CaCu_3Ti_4O_{12})_{0.95}$ composite containing 95 % $CaCu_3Ti_4O_{12}$ below 200 K: the first line has the effective g-factor of approximately 2. The temperature dependences of the position, the linewidth, and the integral intensity of the first line in $(SrFe_{12}O_{19})_{0.05}(CaCu_3Ti_4O_{12})_{0.95}$ are given in Fig. 6 (triangles). Unlike $CaCu_3Ti_4O_{12}$, where the EPR linewidth is independent of the temperature and equal to 200 Oe, the linewidth in $(SrFe_{12}O_{19})_{0.05}(CaCu_3Ti_4O_{12})_{0.95}$ decreases from 1800 to 500 Oe in the temperature range from 100 to 300 K. This indicates a considerable effect of local magnetic fields created by $SrFe_{12}O_{19}$ particles. The maximum of the integral intensity of the first line at $g \sim 2$ is observed at the temperature of about 175 K (see Fig. 6c, triangles). The second line refers to $SrFe_{12}O_{19}$ particles and has a ferromagnetic nature (see Fig. 7). It is logical to assume that the most probable origin of the first line above 200 K is the superparamagnetic behavior of ferrimagnetic $SrFe_{12}O_{19}$ microparticles with $CaCu_3Ti_4O_{12}$ "shells". The larger fraction of strontium hexaferrite in the form of a cylinder is surrounded by CCTO (Fig. 2) and forms the intergrowth elements. Figure 7 shows spectra of the initial CCTO and SFO compounds and the $(SrFe_{12}O_{19})_{0.05}(CaCu_3Ti_4O_{12})_{0.95}$ composite. It can be seen that two lines from $SrFe_{12}O_{19}$ and a broadened line from $CaCu_3Ti_4O_{12}$ overlap in the composite at 100 K.

Temperature dependences of the magnetic resonance spectra of $SrFe_{12}O_{19}$, which were used for the synthesis of composites, in the temperature range 100–300 K are presented in Fig. 5c. The magnetic resonance field, the linewidth, and the integral intensity are shown in Fig. 6 (circles). The behav-

ior of the temperature dependences of the position, linewidth, and intensity of the magnetic resonance line in $SrFe_{12}O_{19}$ were changed in the temperature near 200 K. We assume that the ordering of one of the sublattices of iron ions occurs at this temperature, as is indicated by steps in the temperature dependence of the magnetization of $SrFe_{12}O_{19}$ (see Fig. 4*b*). We note that below this temperature, the EPR lines in the $(SrFe_{12}O_{19})_{0.05}(CaCu_3Ti_4O_{12})_{0.95}$ composite split (see Fig. 5*b*).

4. CONCLUSIONS

The magnetic resonance spectra of $(SrFe_{12}O_{19})_{0.05}(CaCu_3Ti_4O_{12})_{0.95}$ composite were measured in the X-band in the temperature range 100–300 K. It is shown that the ferromagnetic "core" $SrFe_{12}O_{19}$ in the $(SrFe_{12}O_{19})_{0.05}(CaCu_3Ti_4O_{12})_{0.95}$ composite polarizes spins of copper ions at the core–shell interface, forming a single-domain particle, which manifests superparamagnetic properties in the magnetic resonance spectrum in the temperature range 200–300 K. The magnetic phase transition occurs in strontium hexaferrite at the temperature of 200 K, one of the sublattices of spins of the iron ion is ordered antiferromagnetically with respect to others. As a result, ferromagnetic correlations at the core–shell interface $(SrFe_{12}O_{19})_{0.05}(CaCu_3Ti_4O_{12})_{0.95}$ are destroyed at temperatures below 200 K. The phase separation into the ferrimagnetic "core" $SrFe_{12}O_{19}$ and the paramagnetic "shell" $CaCu_3Ti_4O_{12}$ occur gradually in the wide temperature interval from 200 to 25 K due to the different sizes of $SrFe_{12}O_{19}$.

We are grateful to the Ministry of Education and Science of the Russian Federation. T. I. Ch. acknowledges support of the Russian Foundation for Basic Research (project №14-03-00103). I. V. Ya. acknowledges support of the Russian Foundation for Basic Research (project №16-32-00660). Powder diffraction patterns and temperature dependences of the magnetization were measured using the equipment of the Federal Center of Collective Usage of Kazan Federal University. The X-ray fluorescence analysis was performed in the Institute of Geology and Petroleum Technologies of Kazan (Volga region) Federal University.

REFERENCES

1. S. A. Gridnev, Yu. E. Kalinin, A. V. Sitnikov, and O. Stogney, *Nonlinear Phenomena in Nano- and Micro-Heterogeneous Systems*, Binom. Knowledge Laboratory, Moscow (2012) (in Russian).

2. S. E. Kushnir, A. I. Gavrilov, P. E. Kazin, A. V. Grigorieva, Y. D. Tretyakov, and M. Jansen, J. Mater. Chem. **22**, 18893 (2012).

3. Thi Minh Hue Dang, Viet Dung Trinh, Doan Huan Bui, Manh Huong Phan, and Dang Chinh Huynh, Adv. Nat. Sci.: Nanosci. Nanotechnol. **3**, 025015 (1-7) (2012).

4. Jihoon Park, Yang-Ki Hong, Seong-Gon Kim, Sungho Kim, Laalitha S. I. Liyanage, Jaejin Lee, Woncheol Lee, Gavin S. Abo, Kang-Heon Hur, and Sung-Yong An, J. Magn. Magn. Mater. **355**, 1 (2014).

5. Yu. V. Kabirov, V. G. Gavrilyachenko, A. A. Klenushkin, and E. V. Chebanova, Engineering J. of Don **3**, №3 (2014).

6. M. A. Subramanian, Dong Li, N. Duan, B. A. Reisner, and A. W. Sleight, J. Sol. St. Chem. **151**, 323 (2000).

7. P. Linkenheimer, S. Krohns, S. Riegg, S. G. Ebbinghaus, A. Reller, and A. Loidl, Eur. Phys. J. Special Topics **180**, 61 (2010).

8. M. C. Mozzati, C. B. Azzoni, D. Capsoni, M. Bini, and V. Massarotti, J. Phys. Condens. Matter **15**, 7365 (2003).

9. M. A. Pires, C. Israel, W. Iwamoto, R. R. Urbano, O. Agüero, I. Torriani, C. Rettori, P. G. Pagliuso, L. Walmsley, Z. Le, J. L. Cohn, and S. B. Oseroff, Phys. Rev. B **73**, 224404 (2006).

10. R. M. Eremina, I. I. Fazlizhanov, I. V. Yatsyk, K. R. Sharipov, A. V. Pyataev, H.-A. Krug von Nidda, N. Pascher, A. Loidl, K. V. Glazyrin, and Ya. M. Mukovskii, Phys. Rev. B **84**, 064410 (2011).

11. C. M. Fang, F. Kools, R. Metselaar, G. De With, and R. A. de Groot, J. Phys.: Condens. Matter **15**, 6229 (2003).

12. M. Morin, A. Scaramucci, M. Bartkowiak, E. Pomjakushina, G. Deng, D. Sheptyakov, L. Keller, J. Rodriguez-Carvajal, N. A. Spaldin, M. Kenzelmann, K. Conder, and M. Medarde, Phys. Rev. B **91**, 064408 (2015).

13. A. Gruskova, V. Jancarik, J. Slama, and M. Usakova, Acta Phys. Polon. A **113**, 557 (2008).